SMALL-ION AND NANO-AEROSOL PRODUCTION DURING CANDLE BURNING: SIZE DISTRIBUTION AND CONCENTRATION PROFILE WITH TIME

Matthew D. Wright, A. Peter Fews, Paul A. Keitch and Denis L. Henshaw
H. H. Wills Physics Laboratory
University of Bristol
Tyndall Avenue
Bristol
BS8 1TL

This work was supported by CHILDREN with LEUKAEMIA, registered charity No. 298405 (U.K.). Address correspondence to Matthew Wright, H. H. Wills Physics Laboratory, University of Bristol, Tyndall Avenue, Bristol, BS8 1TL, U.K. E-mail: mw0640@bristol.ac.uk

Abstract

The characteristics of small-ions and aerosols in the diameter range 0.4 nm to 1.1 μm, produced during burning of paraffin wax tea-light candles, were investigated using a custom-built aspiration condenser ion mobility spectrometer (ACIMS) and a sequential mobility particle sizer and counter (SMPS+C) system. Peaks in the number concentration were observed at diameters 10 - 30 nm and 100 - 300 nm, consistent with 'normal' and 'sooting' burn modes. In addition, a smaller mode in the size range 2.5 - 9 nm was observed, interpreted as a soot-precursor species. When a fan was placed behind the burning candle a 'modified small-ion' signal was seen at sizes 1.1 - 2.0 nm. This was not observed without the fan present or when a lamp chimney was used. During burning, aerosol concentration was elevated and small-ion counts were low. However after extinction of the flame, this trend was reversed and the number of small-ions increased to levels higher than those observed prior to burning, remaining so for several hours.

Introduction

There has been much concern over the role of ultrafine particles (UFPs) and nano-aerosols in promoting adverse human respiratory and cardiovascular health effects upon inhalation (Seaton et al., 1995; Donaldson et al., 1998; Lighty et al., 2000; Oberdörster, 2005; Maynard and Kuempel, 2005). It is well established that combustion sources produce large amounts of UFP matter. An important mechanism for causation of health problems by UFPs is pulmonary inflammation via oxidative stress (Donaldson et al., 1998; Li et al., 2003). Particles in the UFP size range are more likely to penetrate deeper into the lung, where this mechanism acts (ICRP, 1994). The proposed dominant metric for determining the magnitude of the effect is total particulate surface area (Stoeger et al., 2006; Brown et al., 2001). UFPs have a larger specific surface area (surface area per unit mass) than their larger counterparts, resulting in a greater dose per unit particulate mass. Oberdörster (2000) exposed rats to 50 μg m^{-3} polytetrafluoroethylene (PTFE) via inhalation and found that larger, older PTFE particles (median diameter 132.4 nm) produced lower toxicity and fatality rates than those from smaller particles (median diameter 20.3 nm). Similarly, Brown et al. (2001) observed size dependency on the inflammatory effects of inhalation of polystyrene.

Several studies have demonstrated the existence of a very small species (< 10 nm) produced under various combustion conditions, including open flames and combustion engines, using different measurement methods (Grotheer et al., 2004; Sgro et al., 2003; Cecere et al., 2002; Apicella et al., 2002; Shi et al, 2001; Dobbins et al., 1998). The properties of this 'soot precursor' species are distinct from those of soot (> 10 nm) and they have been detected in flames independently of soot formation (Grotheer et al., 2004). Most importantly from a health perspective, their coagulation coefficients may be several orders of magnitude below those of soot and that expected from the gas kinetic limit for their size (D'Alessio et al., 2005), with a correspondingly longer lifetime and increased likelihood of emission from combustion systems into the atmosphere. Indeed, Shi et al. (2001) have observed a significant number of particles of size < 10 nm both 4 m upwind and more than 25 m downwind of a major road in Birmingham, U.K. They also modelled the coagulation of these particles and showed that the particle number concentration of 3 - 9 nm particles may decrease by only 25% after 20 minutes, using observed data as input parameters for their model. These particles are also partially water-soluble (Sgro et al., 2003; Cecere et al., 2002). Upon inhalation, particles of this size become increasingly likely to deposit in the extrathoracic region and not to penetrate into the lung. However recent work suggests there may be an extrapulmonary mechanism by which particles deposited in this region may pass directly into the central nervous system via the olfactory bulb, circumventing the blood-brain barrier and causing attendant health effects (Oberdörster, 2004).

Indoor combustion sources may contribute significantly to health effects. Previous work has investigated emissions from cooking (Li et al., 1993; Raiyani et al., 1993), domestic heating (Burtscher et al., 1986; Oanh et al., 1999; Przybilla et al., 2002), tobacco smoke, natural gas, propane and candle flames (Huynh et al., 1991; Li and Hopke, 1993; Murr et al., 2004) and incense and mosquito coil smoke (Huynh et al., 1991; Li and Hopke, 1993; Mannix at al., 1996). Smouldering sources such as sidestream tobacco smoke and incense burning produce particles in the size range 100 - 700 nm, with a peak at 200 - 300 nm, whereas particles produced in flames are smaller, in the range 10 - 100 nm with a peak around 30 - 40 nm (Karasev et al., 2004; Li and Hopke, 1993; Mulholland and Ohlemiller, 1982). Several case studies have investigated the contributions to indoor submicron and ultrafine particles from various sources. Abt et al. (2000) identified cooking as the primary indoor source of particles of size 20 - 500 nm in urban Boston, and Matson (2005) concluded that for residential buildings in rural and urban Scandinavia, peak indoor particle concentrations were associated mainly with indoor sources rather than transport of particles inside from outdoors, making direct reference to cooking and candle burning.

Ion emission from flames has been observed and utilised in several early experiments investigating atmospheric electrical properties, for example in the measurements of atmospheric potential gradient by Volta in the late 18th Century and Kelvin in the mid-19th Century. Later, McClelland (1898) undertook studies of the electrical properties of ions produced in flames. Zeleny (1900) enhanced the coaxial condenser system initially used by McClelland for his work on ions produced in gases by X-rays. Further details of these and other early studies can be found in a review on the history of electrical aerosol measurements by Flagan (1998). Several reviews of the literature on ionisation in flames and its measurement have been produced, see for example Fialkov (1997). Charge production in combustion is thought to proceed mainly by chemi-ionisation and in hydrocarbon flames is bipolar in nature. It is predicted that charged particles are more likely than their uncharged counterparts to deposit in the lung due to image charge effects (Cohen et al., 1998). Increased deposition of a population of singly-charged particles over those

at room temperature equilibrium charge (charge-neutralised) distribution was observed by Cohen et al. (1998) for 20 nm and 125 nm particles (ratio of deposition efficiencies 3.4 ± 0.3 and 2.3 ± 0.3 respectively). Thus, should a person be present in a room with a continuous source of charged aerosols (where any increased rate of removal of particles due to additional charge is balanced or outweighed by particle production), a higher dose may be received not only because of any increased concentration but additionally due to increased charge. Burtscher et al. (1986) concluded that the charge distribution depends strongly on the combustion material and can remain highly charged compared to the room temperature equilibrium for a considerable time.

Candles are unlikely to be the primary source of combustion aerosols in most households but for those in which candle burning takes place they may account for a significant proportion of indoor aerosol concentration. In addition, candle burning may be used as a cheap standard source of polydisperse aerosols in the UFP size range which is broadly representative of hydrocarbon laminar diffusion flames and for these reasons it is important to have knowledge of the characteristics of these particles. Li and Hopke (1993) observed a geometric mean particle diameter of 37 nm for particles produced during candle burning. Fine et al. (1999) conducted a study of the size distribution and chemical composition of combustion products from paraffin and beeswax candles and observed two burning modes, a 'normal' mode with a peak in concentration at 50 nm, and a 'sooting' mode with additional particle production at larger diameters leading to a bimodal size distribution. However, these studies reported only sizes down to 10 nm. Reported aerosol concentrations due to candle burning in the literature vary, probably by virtue of differing experimental conditions. For example, Matson (2005) found that UFP concentration increased from under 3,000 particles cm^{-3} to a peak of 15,000 particles cm^{-3} for one candle burning event in a residential building whereas Afshari et al. (2005) obtained a maximum concentration of 241,000 particles cm^{-3} for candles burning in a small enclosed chamber. Previous work has also investigated burning of candles of different composition, for example soybean oil (Rezaei et al., 2002) and citronella candles (LaRosa et al., 2002).

This work investigates the size distributions and number concentrations of small-ions and nano-aerosols, in the size range 0.4 nm to 1.1 μm, produced during candle burning. It is, to our knowledge, the first such work to examine particle production from candle flames to such small sizes, and to detect particles in the soot precursor size range from such a source.

Materials and methods

Small-ion and nano-aerosol mobility spectra in the diameter range 0.4 nm to around 15 nm were obtained using a custom-built aspiration condenser ion mobility spectrometer (ACIMS), described by Fews et al. (2005), which is based on the ventilated cylindrical capacitor designs of Zeleny (1900) and Gerdien (1905) . In the present paper, the distinction between small-ions and nano-aerosols is defined by mobility, with those particles of mobility greater than 5×10^{-5} m^2 V^{-1} s^{-1} (smaller than ~ 1.8 nm) classified as small-ions and particles of lesser mobility (larger size) classified as nano-aerosols. The ACIMS detects charged particles of different mobilities by drawing air at a fixed flow rate through a cylindrical capacitor. The voltage across the capacitor is cycled stepwise from 0 V to ± 1000 V, such that ions of a given mobility and polarity move in the electric field and are deposited on the inner electrode, where a Keithley 6514 electrometer measures the ion current at each voltage step. Each cycle takes approximately 15 minutes. Raw data from these voltage scans are then deconvolved using a method of maximum entropy (Fews

et al., 2005) to obtain the mobility spectra. Data from several cycles can be combined prior to analysis to reduce noise, making the deconvolution process more accurate. The mobility limits of the ACIMS (5×10^{-4} to 2.5×10^{-7} $m^2 V^{-1} s^{-1}$) are determined by its geometry, air flow rate and the maximum and minimum applied voltages.

Aerosol size distributions in the range 10 nm to 1.1 μm were determined using a sequential mobility particle sizer and counter (SMPS+C) from Grimm Aerosol Technik comprised of a differential mobility analyser (DMA) and condensation particle counter (CPC). Air is drawn first through a neutraliser (Am-241) to provide a known charge distribution, then through the DMA to select particles of a given mobility range. The CPC then counts the number of particles in each mobility bin and software is used to extract a size distribution from the raw mobility data.

The two measurement devices differ in several important ways. The ACIMS uses an electrometer to detect the current flow from particles deposited on its central electrode and thus measures only the charged fraction of particles, whereas the SMPS+C, used with a neutraliser, measures total particle concentrations. The obtained ACIMS mobility data is related to the size distribution by making the assumption that, for the diameters in question, all the particles measured are singly-charged. No neutraliser is used in the ACIMS, so if a higher proportion of particles are charged, more will be detected. The Keithley 6514 electrometer has a current detection limit of 10^{-17} A, which in conjunction with the ACIMS geometry and flow rates results in a theoretical lower detection limit of 1.5×10^4 ions m^{-3}, although in practice successful resolution of such a small signal would not be achieved. The CPC used in the SMPS+C system has a resolution of 2×10^5 particles m^{-3} and for particles of diameter > 10 nm has ~ 100% counting efficiency.

Mobility, mass and diameter are evaluated by application of Chapman-Enskog kinetic theory (Chapman and Cowling, 1970) which includes the effects of direct coulomb interaction, image charge interaction and a Lennard-Jones interatomic potential (Fews, 2001, following Tammet, 1995). The parameters within this model were chosen by fitting to experimental data. Particles are assumed to be spherical with a density of 1240 kg m^{-3}. The masses and diameters thus obtained are consistent with expected values (Chapman and Cowling, 1970).

Experimental work was carried out in a room of approximate volume 54 m^3, where draughts were minimised but which was not environmentally enclosed, located in central Bristol, U.K. The air exchange rate of the room was not determined. Unscented petroleum wax based 'tea-light' candles were used throughout the study. Candles were located at a distance of 1.8 m from the measurement devices. Beginning in the mid-morning, several hours of measurements were taken, in order to establish a background ion/aerosol size distribution, before lighting the candle in the early afternoon. The candle remained lit for a further period of around 3 h before being extinguished by first blowing out the flame then pinching the smouldering wick with wet fingers. Measurements were then taken overnight to determine the 'recovery' timescale and ion/aerosol profiles. Six runs were completed in total, for two of which the SMPS+C system was not available. On three occasions, a fan was placed behind the burning candle with the intention of reducing the travel time to the measurement apparatus. To investigate the effects of the fan on the flame itself and on the transport of the combustion products, separate runs using the ACIMS were completed with the candle flame shielded from the direct effect of the fan by a lamp chimney, and secondly with the fan pointing in a direction away from the measurement instrumentation.

Measurements were taken overnight without lighting candles as a means of a control and size distribution in the range 10 nm to 1.1 μm was obtained on striking matches, to determine whether any effects observed were due to the candle alone.

Results and discussion

a) Mobility spectra and size distributions - ACIMS

Mobility spectra obtained using data from several voltage scans on the ACIMS are shown in figure 1. Tables 1 and 2 summarise total positively and negatively charged particle counts of both polarities for runs with no fan and with a fan placed behind the burning candle respectively.

Table 1. ACIMS and SMPS+C data for candle burning only.

		ACIMS				SMPS+C	
Date		+ve ions (m^{-3})	-ve ions (m^{-3})	+ve aerosols (m^{-3})	-ve aerosols (m^{-3})	total aerosols (m^{-3})	mean size (nm)
Apr 27 2005	before	$4.65x10^{8}$	$4.20x10^{8}$	$2.37x10^{8}$	$2.53x10^{8}$	N/A	N/A
	during	$1.53x10^{8}$	$1.34x10^{8}$	$4.40x10^{9}$	$4.60x10^{9}$	N/A	N/A
	3h after	$7.35x10^{8}$	$5.54x10^{8}$	$2.09x10^{8}$	$2.21x10^{8}$	N/A	N/A
	9h after	$6.66x10^{8}$	$5.60x10^{8}$	$6.32x10^{7}$	$6.27x10^{7}$	N/A	N/A
May 3 2005	before	$3.94x10^{8}$	$3.15x10^{8}$	$1.40x10^{8}$	$1.45x10^{8}$	$5.57x10^{9}$	43.0
	during	$6.81x10^{7}$	$6.37x10^{7}$	$4.62x10^{9}$	$4.92x10^{9}$	$9.68x10^{9}$	35.7
	3h after	$7.55x10^{8}$	$5.93x10^{8}$	$9.63x10^{7}$	$1.09x10^{8}$	$4.61x10^{9}$	47.1
	9h after	$8.46x10^{8}$	$6.59x10^{8}$	$6.97x10^{7}$	$7.83x10^{7}$	$3.98x10^{9}$	59.9
Jun 1 2005	before	$3.22x10^{8}$	$2.44x10^{8}$	$8.50x10^{7}$	$1.11x10^{8}$	$4.98x10^{9}$	46.5
	during	$1.01x10^{8}$	$8.50x10^{7}$	$3.54x10^{9}$	$3.99x10^{9}$	$9.96x10^{9}$	40.3
	3h after	$9.97x10^{8}$	$7.49x10^{8}$	$6.29x10^{7}$	$6.57x10^{7}$	$2.17x10^{9}$	47.5
	9h after	$6.97x10^{8}$	$4.99x10^{8}$	$5.87x10^{7}$	$7.02x10^{7}$	$1.22x10^{9}$	57.9

Table 2. ACIMS and SMPS+C data for candle burning with fan.

		ACIMS				SMPS+C	
Date		+ve ions (m^{-3})	-ve ions (m^{-3})	+ve aerosols (m^{-3})	-ve aerosols (m^{-3})	total aerosols (m^{-3})	mean size (nm)
Jul 29 2004	before	$1.92x10^{8}$	$1.54x10^{8}$	$1.25x10^{8}$	$1.30x10^{8}$	N/A	N/A
	during	$5.97x10^{8}$	$9.39x10^{8}$	$6.18x10^{9}$	$6.50x10^{9}$	N/A	N/A
	3h after	$5.57x10^{8}$	$4.30x10^{8}$	$5.32x10^{7}$	$5.79x10^{7}$	N/A	N/A
	9h after	$9.15x10^{8}$	$7.40x10^{8}$	$4.89x10^{7}$	$6.30x10^{7}$	N/A	N/A
Jun 7 2005	before	$1.35x10^{8}$	$1.05x10^{8}$	$9.60x10^{7}$	$1.00x10^{8}$	$7.78x10^{9}$	61.3
	during	$1.49x10^{9}$	$1.55x10^{9}$	$3.04x10^{9}$	$3.01x10^{9}$	$2.30x10^{10}$	41.6
	3h after	$1.49x10^{8}$	$1.14x10^{8}$	$6.40x10^{7}$	$5.80x10^{7}$	$5.74x10^{9}$	72.2
	9h after	$1.43x10^{8}$	$1.02x10^{8}$	$7.69x10^{7}$	$8.61x10^{7}$	$7.48x10^{9}$	71.7
Jun 10 2005	before	$2.63x10^{8}$	$2.14x10^{8}$	$1.33x10^{8}$	$1.41x10^{8}$	$7.61x10^{9}$	44.4
	during	$1.48x10^{9}$	$2.37x10^{9}$	$8.34x10^{9}$	$8.17x10^{9}$	$2.07x10^{10}$	33.3
	3h after	$2.87x10^{8}$	$2.27x10^{8}$	$6.91x10^{7}$	$7.05x10^{7}$	$5.71x10^{9}$	50.2
	9h after	$4.34x10^{8}$	$3.49x10^{8}$	$7.49x10^{7}$	$8.17x10^{7}$	$3.56x10^{9}$	53.8

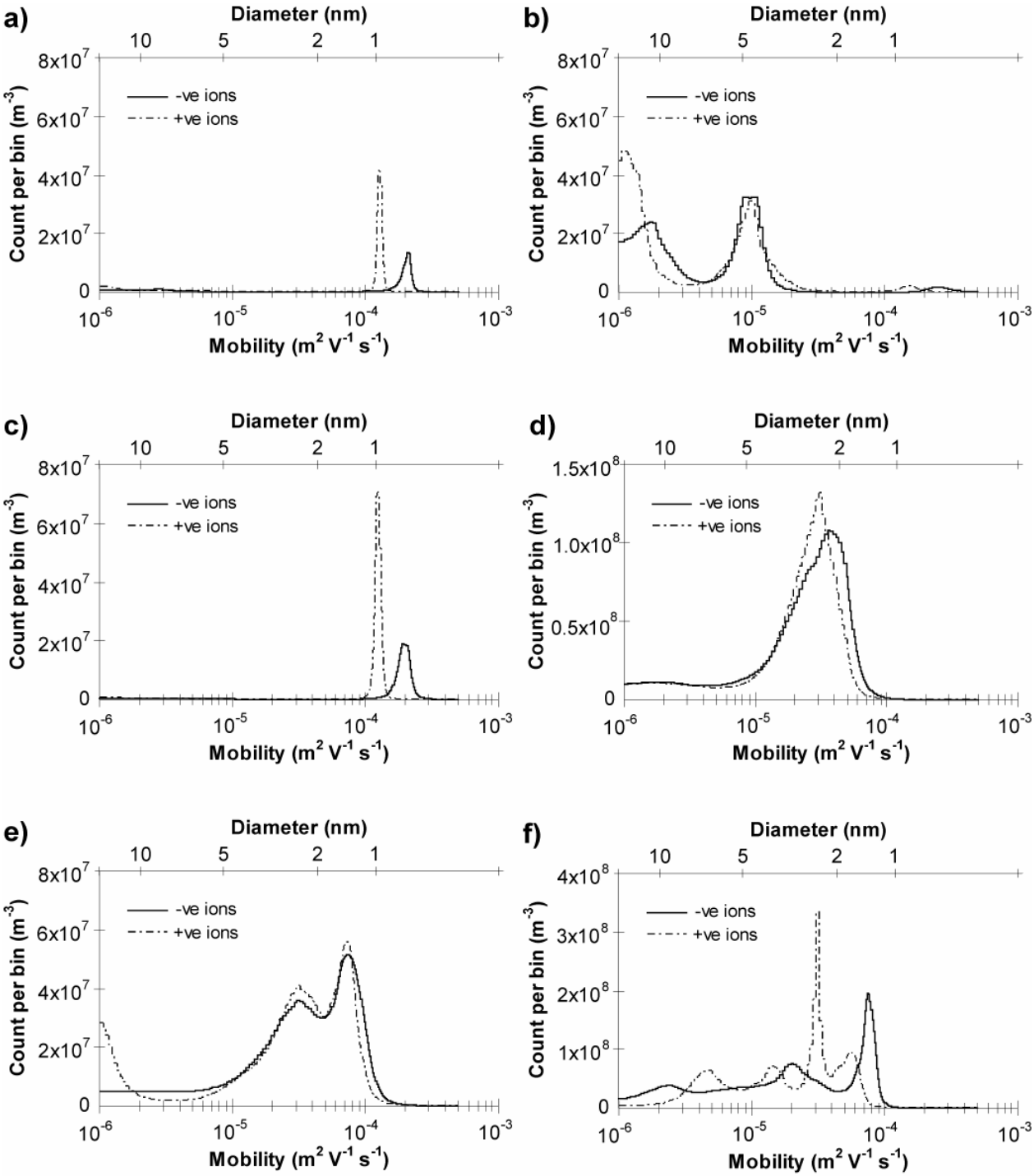

Figure 1. ACIMS mobility spectra obtained a) before lighting candle, b) during candle burning , c) several hours after candle extinguished (all on Jun 1 2005) and d), e), f) during candle burning with fan on Jul 29 2004, Jun 7 2005 and Jun 10 2005 respectively.

Typical indoor air samples produce spectra similar to that seen in figure 1a, which shows atmospheric small-ion peaks at mobilities in the region of 1 - 2 x 10^{-4} m^2 V^{-1} s^{-1} corresponding to 0.6 - 1.0 nm in size, with positive ions being larger and of lower mobility than negative ions. Small numbers of charged aerosols with mobilities < 10^{-5} m^2 V^{-1} s^{-1} are present before the candle was lit but are not present several hours after the candle is extinguished (figure 1b). Candle

burning (figure 1c) produces large numbers of aerosols in the mobility range 10^{-6} to 5 x 10^{-5} m^2 V^{-1} s^{-1}, a size range of around 2.5 - 9 nm, and suppression of small-ions as they attach to these aerosols. Similarly sized species have been reported in several other studies under various combustion conditions (Grotheer et al., 2004; Sgro et al., 2003; Shi et al., 2001). Apicella et al. (2002) detected the presence of at least three classes of species in a premixed laminar ethylene flame, with estimated masses of the order 10^3, 10^5 and 10^6 amu, and suggested the largest two species were very large molecules rather than aggregates of smaller molecules. Since no chemical analysis of the combustion products was undertaken in this study, it is not possible to confirm whether the properties of the species described above are similar to carbonaceous soot or to those of soot precursor particles, which have a lower C/H ratio and lower coagulation rate than carbonaceous soot (D'Alessio, 2005).

When a fan is placed behind the burning candle (figures 1d, 1e and 1f), the spectrum is shifted to higher mobility. It is also important to note the presence of an additional peak at mobilities 5 - 9 x 10^{-5} m^2 V^{-1} s^{-1}, corresponding to an approximate size range 1.1 - 2.0 nm, on two of the three runs. Because this 'modified small-ion' peak is relatively well-defined in comparison to the larger, less mobile particles and is present in addition to this mode, they appear to be a distinctly different species to the normal mode observed without the fan. The number of ions detected in this peak is much greater than the number present in ambient air prior to candle burning, suggesting that they are produced in the flame. The increase in number of particles measured may be due to the presence of a greater concentration of particles, a higher proportion of those particles carrying a charge, or a combination of both.

The fan could affect results in a number of ways, both direct and indirect. Physical disturbance of the flame may introduce cold air, lowering the temperature of the flame, altering the fuel-air ratio and increasing the amount of fuel-air mixing within the flame. This appears to lead to interference with processes such as recombination and oxidation reactions, which would ordinarily act to reduce the number and increase the size of the particles eventually emitted from the flame. Indirect effects could include increased transport rate of combustion products to the detectors or increased coagulation of particles due to turbulence induced by the fan.

The modified small-ion peak was observed in different positions on figures 1e and 1f and on one other occasion (figure 1d) the peak appears to have merged into the 'soot-precursor' peak at mobilities 3 - 5 x 10^{-5} m^2 V^{-1} s^{-1}. The most likely explanation for this is that the fan was positioned slightly differently on each occasion, changing its effect on the flame chemistry and leading to production of particles of differing characteristics. The lowest mobility peaks observed, those in figure 1e, correspond to a mass of approximately 700 - 1500 amu for negative ions and 950 - 1600 amu for positive ions. Dobbins et al. (1998) report PAHs as large as 472 amu as constituents of soot precursor particles from an ethene diffusion flame, but the larger sizes are detected in smaller numbers, suggesting the peaks measured in the present work are not due to individual PAH species such as these. They could be small clusters or groups of 2- or 3-ring aromatic compounds described in previous work (Sgro et al., 2003; Grotheer et al., 2004), possibly also with smaller species which normally comprise the small-ion composition in ambient air weakly bound to them. This may explain the removal of the smaller, more mobile atmospheric ions observed before and several hours after burning.

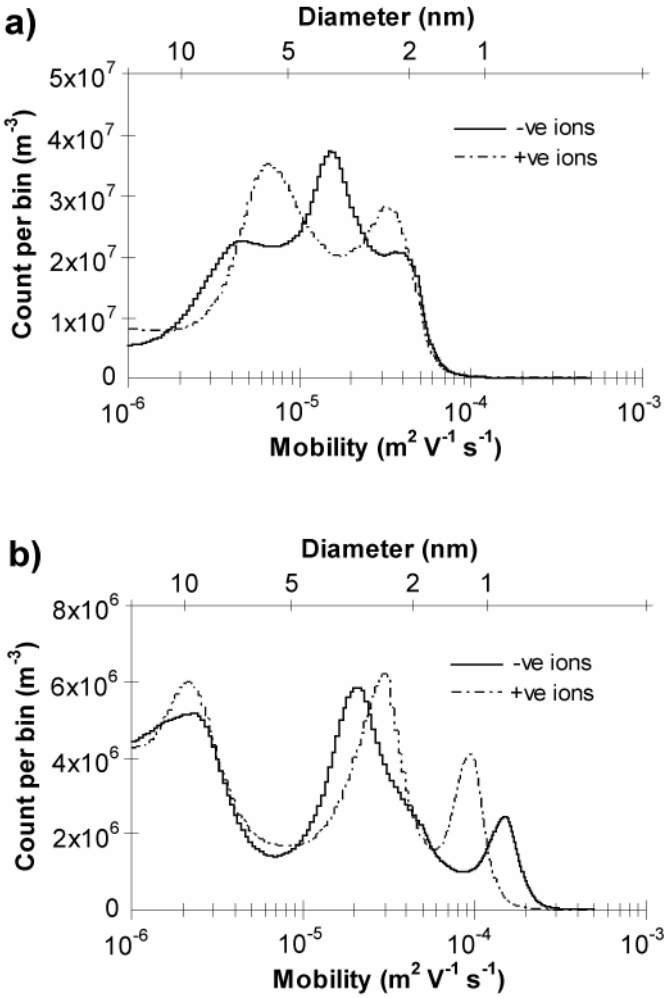

Figure 2. ACIMS mobility spectra obtained during candle burning a) with flame shielded from the fan by a lamp chimney, b) with the fan pointing away from the measurement devices.

Using the lamp chimney (figure 2a) results in a spectrum similar in shape to those without the chimney, but shifted to lower mobility and without the modified small-ion peak observed previously, suggesting the fan has a direct effect on the flame. ACIMS charged nano-aerosol concentration was around 1 x 10^{10} m^{-3}, similar in magnitude to that observed without the lamp chimney. Pointing the fan away from the measurement devices (figure 2b) produces a greater number of aerosols in the size range 7 - 15 nm, with a lesser peak in the smaller size range 2 - 3.5 nm. In addition, the modified small-ion peak is present (at sizes 0.9 nm and 1.1 nm for negative and positive ions respectively), although at much lower concentrations than with the fan directly facing the ACIMS. The ion peak has a mobility between those observed in ambient air and those with the fan directed towards the ACIMS. In addition to removal by attachment to larger aerosol particles, these small-ions may also reduce in size over time by breakdown into smaller groups of ions and molecules. This would result in an increase in mobility and concentration with time until the peaks more closely resemble the pre- and post-burn ambient small ions. ACIMS charged nano-aerosol concentration during burning with the fan pointing away is much lower than is observed without the fan (around 2 x 10^{9} m^{-3} compared with 7 x 10^{9} - 1 x 10^{10} m^{-3} with no fan), which is likely to be a result of increased coagulation and growth above the maximum size range measurable by the ACIMS, due to the forced turbulent flow and increased mixing within the

room induced by the fan. This may not be as important when the fan is directed toward the instrumentation as less time is available for coagulation in the forced flow.

ACIMS data analysis assumes that each particle detected carries a single charge. For the sizes concerned and under ambient conditions, the contribution from multiply-charged particles is negligible. However, during candle burning, charge distribution is not at room temperature equilibrium, therefore the percentage of particles carrying two or more electronic charges may be higher than expected. This problem is exacerbated for the largest particles, which can hold more charge, so the observed count per bin may be overestimated as the measured particle size distribution is shifted to lower diameters.

b) Size distributions - SMPS+C

Typical aerosol size distributions obtained from the SMPS+C are shown in figure 3, and the results show similar trends to those from ACIMS data. All data given in parts b) and c) refer to number concentration of particles. Candle burning produces large numbers of aerosols especially below 50 nm in diameter (peak ~ 20 nm) and use of the fan both increases the number of particles detected and reduces their mean size (peak is shifted below the measurable range of the SMPS+C, < 10 nm). Secondary peaks at larger sizes (~ 200 nm) appear during candle burning both with and without the fan consistent with a sooting mode. These results are broadly consistent with previous studies, see for example Karasev et al. (2004), Fine et al. (1999), Li and Hopke (1993) and Mulholland and Ohlemiller (1982).

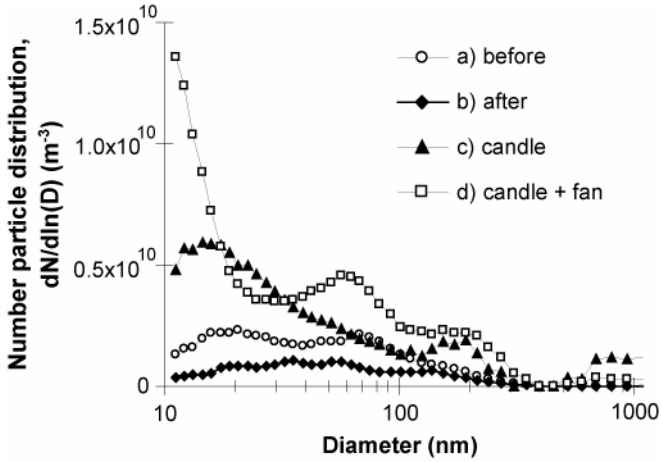

Figure 3. SMPS+C size distributions in the range 10-1000 nm. Data taken from individual runs on Jun 1 2005 (curves a to c) and Jun 10 2005 (curve d).

c) Particle concentration as a function of time

Figure 4 shows typical ACIMS small-ion (~ 0.4 to 1.8 nm) and charged nano-aerosol (~ 1.8 nm to ~ 15 nm) number profiles with time, for positively and negatively charged particles separately. Figure 5 shows typical total number particle counts in the size range 10 nm to 1.1 μm as a function of time obtained using the SMPS+C. Measured concentrations for all runs on both ACIMS and SMPS+C systems, before and during candle burning, and 3 hours and 9 hours after extinguishing, are given in table 1 (without the fan) and table 2 (with the fan).

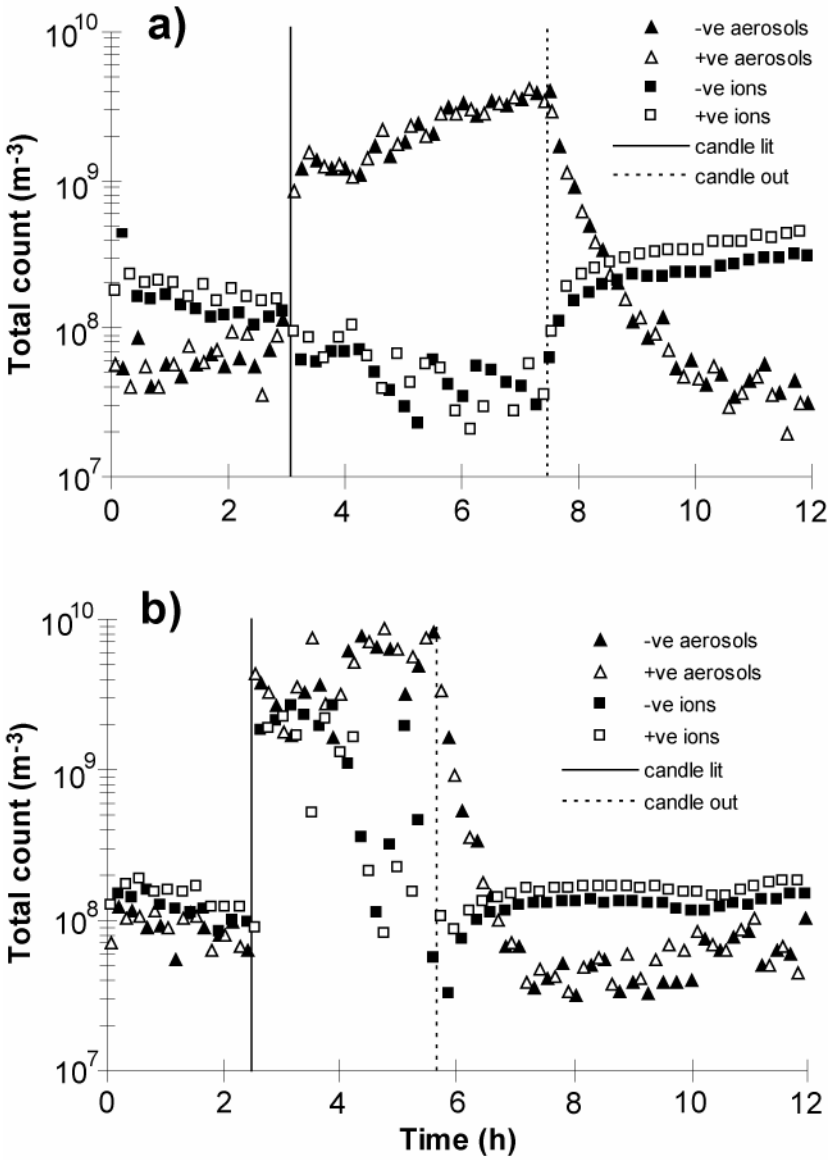

Figure 4. Small-ion and charged nano-aerosol counts obtained from single runs on the ACIMS during a) candle burning on Jun 1 2005, and b) candle burning with fan on Jun 10 2005.

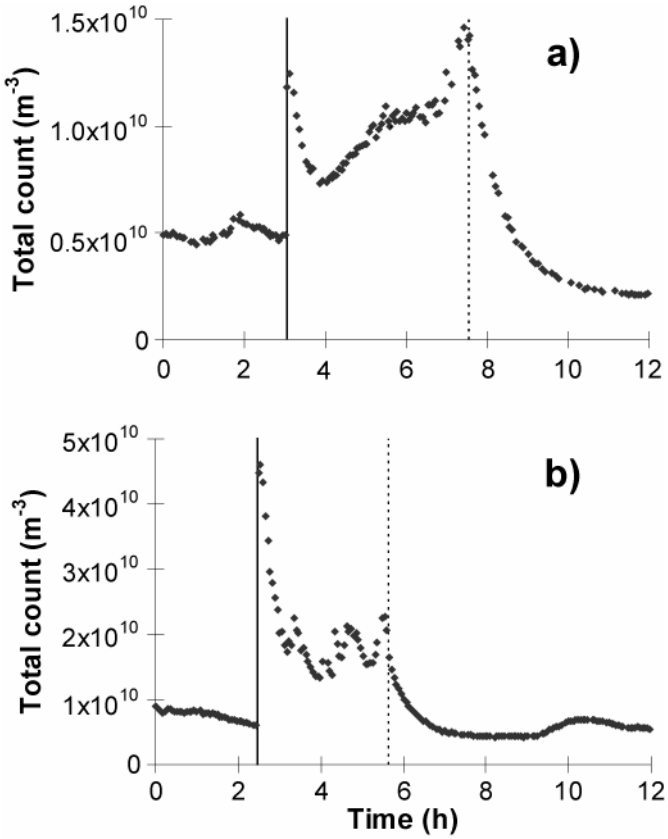

Figure 5. Aerosol counts obtained from single runs on the SMPS+C during a) candle burning on Jun 1 2005, and b) candle burning with fan on Jun 10 2006. The solid vertical lines represent candle lighting and the broken vertical lines when the candle was extinguished.

For the larger aerosols the highest concentrations were generally seen immediately after lighting, but the concentration of the smallest (as measured using the ACIMS) continued to rise after the initial sharp increase. The concentration of charged nano-aerosols was vastly increased during burning. Immediately after lighting and throughout burning, small-ion count is decreased. With higher aerosol concentration, the ion-aerosol attachment rate is much faster than the ion production rate, so rapid depletion of small-ions is expected. Elevated aerosol concentration during burning also raises the coagulation rate of aerosols - for example, in the simple case of a monodisperse aerosol population, coagulation rate is proportional to the square of the number concentration (Hinds, 1982). When the source is then removed by extinguishing the candle, total aerosol mass is no longer increasing and if size growth occurs the number concentration must therefore decrease. Also, larger aerosols are very effective at 'sweeping up' smaller ones - for example, the coagulation rate between 1 μm and 10 nm particles is 25 times that between 10 nm particles alone, and 500 times that between 1 μm particles alone (Hinds, 1982). Number concentration of sub-micron particles is highly dependent on these smaller aerosols and thus can decrease substantially if many large aerosols are present. Candle burning produces a population of particles of size 100 - 300 nm, for which the coagulation coefficients with 10 nm particles are 3 - 8 times that of 10 nm particles alone. Coagulation will also increase the size of some aerosols above the measurable range of the devices, reducing the total number detected.

The modified small-ion peak with the fan is apparent in figure 4b, when a sudden increase in concentration of both positive and negative small ions is seen upon candle lighting. For this particular measurement, however, the concentration appears to drop throughout the candle burning period, concurrently with an increase in nano-aerosol concentration. This would be consistent with production of larger particles in the flame, perhaps by a gradual change in the combustion conditions, or by increased particle growth between production and measurement. There was little evidence of this occurring during other runs with the fan, as the concentration of small-ions remained at a high level and the peak remained at similar mobility throughout candle burning.

In general, an increase in small-ion concentration was observed several hours after extinguishing when compared with background measurements, although the mobilities are similar, suggesting that these are the same ions that are observed in ambient air. This increase continues until steady-state is reached between ion pair production and the slower net rate of removal by ion-aerosol attachment (owing to the decreased aerosol concentration), which in the present study took up to 7 hours after extinguishing when no fan was used (data not shown). A greater concentration of small-ions is observed until aerosol concentration increases to the ambient level observed prior to candle lighting. This usually occurs at the morning rush-hour of the following day. The effect is much more pronounced on weekdays, presumably due to increased traffic volume.

Measured concentration of both small-ions and aerosols in general show greater variability when the fan is present, both during and after candle burning took place. The increase in small-ion concentration after extinguishing was much quicker with the fan, reaching a steady-state within 90 minutes. Aerosols coagulate and are removed from the air much quicker with increased flow and turbulence, facilitating an increase in ion concentration which occurs more quickly than with no forced air flow. Aerosol depletion displays a similar response to use of the fan, with a characteristic depletion half-time of 20 minutes with and 36 minutes without the fan. Afshari et al. (2005) observed similar decay rates for ultrafine and fine particles after candle extinguishing, in a chamber of slightly smaller size (32 m^3) with an air exchange rate of 1.7 ± 0.1 h^{-1}.

Results from the ACIMS and the SMPS+C systems are in good qualitative agreement (tables 1 and 2). Nano-aerosol concentrations in the 1.8 – 15 nm range measured by the ACIMS follow the same pattern as the larger diameters measured by the SMPS+C throughout the candle burning/extinguishing sequence, driven by the production of large numbers of charged particles during candle burning. Without the fan, when aerosol concentrations (as measured by either system) increase, ion concentration drops. Considering the concentrations during and post-burning as a fraction of their values prior to burning, it could be suggested that the greater the increase in aerosols during burning, the greater the drop in ions, and also the stronger the reverse effect that occurs several hours after candle extinction, although further quantitative analysis would require more data. This is less obvious looking at results obtained using the fan, primarily because the additional smaller mode of particles produced contributes to both the aerosol count (> 1.8 nm) and the ‘small ion’ count (< 1.8 nm) of the ACIMS results, and its position varies from run to run. It is also noted that post-burning, when ion concentrations are highest, the size distribution of the aerosols measured using the SMPS+C is shifted to larger diameters and their mean size increases (tables 1 and 2).

d) Other measurements

Urban aerosol counts both indoors and outdoors fluctuate naturally on a daily basis and are different on weekends to weekdays. In the present work, a typical midweek indoor minimum was reached around 2 a.m. at 2 x 10^9 particles m^{-3}, rising to a morning peak at around 9 a.m. of 5 x 10^9 particles m^{-3}. However, these variations are negligible compared to the concentrations reached during candle burning, especially when experiments are conducted during a period of the day when natural variation is ordinarily not of the magnitude described above.

Lighting a single match caused a peak of around double the total background concentration when measured by the SMPS+C. A large peak in the size distribution at ~ 100 nm was observed, although a general increase in number concentration of around 20% of all sizes up to ~ 300 nm was also seen within 3 minutes of striking. The effect appears to be significantly diluted within one hour, although it could still contribute to the initial peak and subsequent drop in aerosol concentration observed upon lighting the candle.

e) Potential health implications

SMPS+C data show an increase in total aerosol concentration, whereas ACIMS data show a much greater measured number of charged aerosols during burning. However, with the current experimental setup, it is not possible to determine whether this is due to increased concentration, or because an increased proportion of the particles carry charge. In the ICRP model of particle deposition in the lung (ICRP, 1994), deposition is expressed as fraction of inhaled particles, therefore a doubling of aerosol concentration results in a doubling of received dose. Additional charge can increase the fraction of particles retained in the lung, but increased dose is likely to be determined by the increased concentration of particles produced during burning rather than their charge. This is most obvious when considering the smallest particles, diameters < 10 nm, which have deposition fractions > 95 %, regardless of their charge state. If the 20- to 30-fold increase in nano-aerosols (~ 1.8 - 15 nm diameter) measured by the ACIMS during candle burning (Table 1) is due mainly to increased concentration, rather than elevated charge state, then anyone present in the same room as a burning candle will receive a vastly increased inhaled dose. The extent of this effect could be quantified if the charge state is known, for example by comparison with total aerosol concentration in the same size range. This was not undertaken in the present work because the overlap of the two devices was only in the limited diameter range 10 - 15 nm.

Conclusions

Characterisation of the size distribution in the size range ~ 0.4 nm to 1.1 μm and evolution of the number concentration profile of combustion products from paraffin wax tea-light candles was undertaken.

Candle burning produces large numbers of particles in the size range 10 - 30 nm, where particle number concentration is increased by 2 - 3 times above background levels prior to burning, and a secondary peak at 100 - 300 nm attributed to sooting during inefficient burning. These results are in broad agreement with previous work on the size distribution of combustion products. The present study also found evidence for a smaller mode, with a peak in concentration at diameters 2.5 - 9 nm, which is interpreted as the soot precursor particle species reported in the literature. A

'modified small-ion' signal at diameters 1.1 - 2.0 nm was found but was only present when a fan was placed behind the burning candle. It is postulated that the structure of this species is distinct from the larger species detected, and that its presence is linked with disturbance of the flame by the fan, as the peak did not appear when a lamp chimney was used to shield the flame.

Atmospheric small-ions were depleted during burning to around 20% of normal concentrations because of attachment to increased numbers of aerosols produced in the flame, but increased to higher than normal levels several hours after the flame was extinguished. Aerosol concentrations were elevated during burning, but dropped below background concentrations after extinguishing due to an increased coagulation rate in the particle-rich environment with no source of new aerosols. This leads to less ion-aerosol attachment and consequently gives rise to the aforementioned increase in small-ion concentration. The concentration of small-ions reached a steady state several hours after extinguishing, however this process was hastened greatly by use of a fan in the room. These results are heavily dependent on the conditions within the room at the time in which the experiment took place.

Although not the major source of indoor air pollution in most environments, a vastly increased inhaled dose of nano-aerosols from combustion could be received by anyone present in a typical domestic room containing a burning candle. Further work is required to characterise the charge state of the smallest particles produced in candle flames and to determine the extent of such increased deposition of combustion particles in the lung.

References

Abt, E., Suh, H. H., Allen, G. and Koutrakis, P. (2000). Characterization of indoor particle sources: a study conducted in the metropolitan Boston area, *Env. Health Perspect.* 108:35-44.

Afshari, A., Matson, U. and Ekberg, L. E. (2005). Characterization of indoor sources of fine and ultrafine particles: a study conducted in a full-scale chamber, *Indoor Air* 15:141-150.

Apicella, B., Ciajolo, A., Suelves, I., Morgan, T. J., Herod, A. A. and Kandiyoti, R. (2002). Structural characterization of products from fuel-rich combustion: an approach based on size exclusion chromatography, *Combust. Sci. Technol.* 174:345-359.

Brown, D. M., Wilson, M. R., MacNee, W., Stone, V. and Donaldson, K. (2001). Size-dependent proinflammatory effects of ultrafine polystyrene particles: a role for surface area and oxidative stress in the enhanced activity of ultrafines, *Toxicol. Appl. Pharmacol.* 175:191-199.

Burtscher, H., Reis, A. and Schmidt-Ott, A. (1986). Particle charge in combustion aerosols, *J. Aerosol Sci.* 17:47-51.

Cecere, D., Sgro, L. A., Basile, G., D'Alessio, A. and D'Anna, A. (2002). Evidence and characterization of nanoparticles produced in nonsooting premixed flames, *Combust. Sci. Technol.* 174:377-398.

Chapman, S. and Cowling, T. G. (1970). *The mathematical theory of non-uniform gases*. Cambridge University Press.

Cohen, B. S., Xiong, J. Q., Fang, C.-P. and Li, W. (1998). Deposition of charged particles on lung airways, *Health Physics* 74:554-560.

D'Alessio, A., Barone, A. C., Cau R., D'Anna, A., Minutolo, P. (2005). Surface deposition and coagulation efficiency of combustion generated nanoparticles in the size range from 1 to 10 nm, *Proc. Combust. Inst.* 30(2):2595-2603.

Dobbins, R. A., Fletcher, R. A. and Chang, H.-C. (1998). The evolution of soot precursor particles in a diffusion flame, *Combust. Flame* 115:285-298.

Donaldson, K., Li, X. Y. and MacNee, W. (1998). Ultrafine (nanometre) particle mediated lung injury, *J. Aerosol Sci.* 29:553-560.

Fews, A. P. (2001). Internal report, University of Bristol.

Fews, A. P., Holden, N. K., Keitch, P. A. and Henshaw, D. L. (2005). A novel high-resolution small-ion spectrometer to study nucleation of aerosols in ambient indoor and outdoor air, *Atmos. Res.* 76:29-48.

Fialkov, A. B. (1997). Investigations on ions in flames, *Prog. Energy Combust. Sci.* 23:399-528.

Fine, P. M., Cass, G. R. and Simoneit, B. R. T. (1999). Characterization of fine particle emissions from burning church candles, *Environ. Sci. Technol.* 33:2352-2362.

Flagan, R. C. (1998). History of electrical aerosol measurements, *Aerosol Sci. Tech.* 28:301-380.

Gerdien, H. (1905). Demonstration eines apparates zur absoluten Messung der elektrischen Leitfahigkeit der Luft, *Phys. Z.* 6:800-801.

Grotheer, H.-H., Pokorny, H., Barth, K.-L., Thierley, M. and Aigner, M. (2004). Mass spectrometry up to 1 million mass units for the simultaneous detection of primary soot and of soot precursors (nanoparticles) in flames, *Chemosphere* 57:1335-1342.

Hinds, W. C. (1982). *Aerosol Technology*. John Wiley & Sons, New York.

Huynh, C. K., Savolainen, H., Vu-Duc, T., Guillemin, M. and Iselin, F. (1991). Impact of thermal proofing of a church on its indoor air quality: the combustion of candles and incense as a source of pollution, *Sci. Total Environ.* 102:241-251.

International Commission on Radiological Protection (ICRP) (1994). Human Respiratory Tract Model For Radiological Protection. ICRP Publication 66, Pergamon Press.

Karasev, V. V., Ivanova, N. A., Sadykova, A. R., Kukhareva, N., Baklanov, A. M., Onischuk, A. A., Kovalev, F. D. and Beresnev, S. A. (2004). Formation of charged soot aggregates by combusion and pyrolysis: charge distribution and photophoresis, *J. Aerosol Sci.* 35:363-381.

LaRosa, L. E., Buckley T. J. and Wallace, L. A. (2002). Real-time indoor and outdoor measurements of black carbon in an occupied house: an examination of sources, *J. Air Waste Manage. Assoc.* 52:41-49.

Li, C.-S., Lin, W.-H. and Jenq, F.-T. (1993). Size distributions of submicrometer aerosols from cooking, *Environ. Int.* 19:147-154.

Li, N., Sioutas, C., Cho, A., Schmitz, D., Misra, C., Sempf, J., Wang, M., Oberley, T., Froines, J. and Nel, A. (2003). Ultrafine particulate pollutants induce oxidative stress and mitochondrial damage, *Environ. Health Perspect.* 111:455-460.

Li, W. and Hopke, P. K. (1993). Initial size distributions and hygroscopicity of indoor combustion aerosol particles, *Aerosol Sci. Tech.* 19:305-316.

Lighty, J. S., Veranth, J.M. and Sarofim, A. F. (2000). Combustion aerosols: factors governing their size and composition and implications to human health, *J. Air Waste Manage. Assoc.* 50:1565-1618.

McClelland, J. A. (1898). On the conductivity of the hot gases from flames, *Phil. Mag.* 46:29-42.

Mannix, R. C., Nguyen, K. P., Tan E. W., Ho, E. E. and Phalen, R. F. (1996). Physical characterization of incense aerosols, *Sci. Total Environ.* 193:149-158.

Matson, U. (2005). Indoor and outdoor concentrations of ultrafine particles in some Scandinavian rural and urban areas, *Sci. Total Environ.* 343:169-176.

Maynard, A. D. and Kuempel, E. D. (2005). Airborne nanostructured particles and occupational health, *J. Nanoparticle Res.* 7:587-614.

Mulholland, G. and Ohlemiller, T. J. (1982). Aerosol characterization of a smoldering source, *Aerosol Sci. Tech.* 1:59-71.

Murr, L. E., Bang, J. J., Esquivel, E. V., Guerrero, P. A. and Lopez, D. A. (2004). Carbon nanotubes, nanocrystal forms, and complex nanoparticle aggregates in common fuel-gas combustion sources and the ambient air, *J. Nanoparticle Res.* 6:241-251.

Oanh, N. T. K., Reutergårdh, L. B. and Dung, N. T. (1999). Emission of polycyclic aromatic hydrocarbons and particulate matter from domestic combustion of selected fuels, *Environ. Sci. Technol.* 33:2703-2709.

Oberdörster, G. (2000). Toxicology of ultrafine particles: *in vivo* studies, *Phil. Trans. R. Soc. Lond. A* 358:2719-2740.

Oberdörster, G., Sharp, Z., Atudorei, V., Elder, A., Gelein, R., Kreyling, W. and Cox, C. (2004). Translocation of inhaled ultrafine particles to the brain, *Inhal. Toxicol.* 16:437-445.

Oberdörster, G., Oberdörster, E. and Oberdörster, J. (2005). Nanotoxicology: An emerging discipline evolving from studies of ultrafine particles, *Environ. Health Perspect.* 113:823-839.

Przybilla, K., Burtscher, H., Qian, Z. and Matter, U. (2002). Ultrafine particle emissions of residential oil burners: influence of burner type, fuel and additives, *Combust. Sci. Technol.* 174:49-66.

Raiyani, C. V., Shah, S. H., Desai, N. M., Venkaiah, K., Patel, J. S., Parikh, D. J. and Kashyap, S. K. (1993). Characterization and problems of indoor pollution due to cooking stove smoke, *Atmos. Environ.* 27A:1643-1655.

Rezaei, K., Wang, T. and Johnson, L. A. (2002). Combustion characteristics of candles made from hydrogenated soybean oil, *J. Am. Oil Chem. Soc.* 79:803-808.

Seaton, A., MacNee, W., Donaldson, K. and Godden, D. (1995). Particulate air pollution and acute health effects, *Lancet* 345:176-178.

Sgro, L. A., Basile G., Barone A. C., D'Anna, A., Minutolo, P., Borghese, A. and D'Alessio, A. (2003). Detection of combustion formed nanoparticles, *Chemosphere* 51:1079-1090.

Shi, J. P., Evans, D. E., Khan, A. A. and Harrison, R. M. (2001). Sources and concentration of nanoparticles (< 10 nm diameter) in the urban atmosphere, *Atmos. Environ.* 35:1193-1202.

Stoeger, T., Reinhard, C., Takenaka, S., Schroeppel, A., Karg, E., Ritter, B., Heyder, J. and Schulz, H. (2006). Instillation of six different ultrafine carbon particles indicates a surface area threshold dose for acute lung inflammation in mice, *Env. Health Perspect.* 114:328-333.

Tammet, H. (1995). Size and mobility of nanometer particles, clusters and ions, *J. Aerosol Sci.* 26:459-475.

Zeleny, J. (1900). The velocity of ions produced in gases by Röntgen rays, *Phil. Trans. Roy. Soc. London A* 195:193-234.